Multistatic Array Sampling Scheme for Fast Near-Field Image Reconstruction

William F. Moulder, James D. Krieger, Denise T. Maurais-Galejs, Huy T. Nguyen, and Jeffrey S. Herd

***Abstract*—A novel multistatic array topology and image reconstruction algorithm for fast 3D near field microwave imaging are presented. Together, the techniques allow for hardware efficient realization of an electrically large aperture and video-rate image reconstruction. The array topology samples the scene on a regular grid of phase centers, using a tiling of Boundary Arrays (BAs). Following a simple correction, the sampled data can then be processed with the well-known and highly efficient monostatic FFT imaging algorithm. In this work, the approach is described and validated experimentally with the formation of high quality microwave images. It is further shown that the scheme is more than two orders of magnitude more computationally efficient than the prevailing backprojection method, and that a cluster of four COTS GPUs can render a 3D image of a human-sized scene in $0.048sec - 0.101sec$.**

***Index Terms*—Microwave imaging, multistatic radar, Fast Fourier Transform (FFT).**

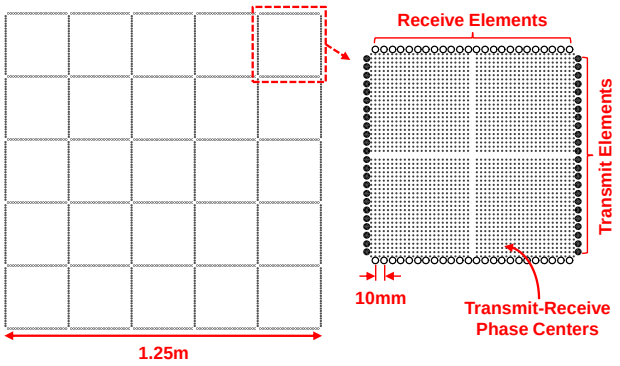

Fig. 1. 1.25m example of multistatic array topology for fast near-field imaging.

I. Introduction

Near-field microwave imaging is a non-ionizing and cost effective sensing modality for variety of applications, including Non-Destructive Evaluation (NDE) [1], medical diagnostics [2], and detection of concealed weapons [3]–[5]. In the latter application, a need exists for a practical system that can image subjects in high foot traffic environments, such as mass transit systems, stadiums, and large public events. In order to handle a potentially constant stream of subjects in motion, the system would need to measure a subject very quickly (on the order of 10's of milliseconds), and reconstruct microwave images of a subject at video rate.

These system requirements present two major challenges. The first challenge is a cost effective realization of an electrically large antenna array. The fast acquisition requirement implies that the system must be fully electronic (e.g., it samples the scene with no moving sensors). Furthermore, for proper near-field illumination of a human subject, the array must be roughly the size of the subject (1-2m). For a high resolution system operating in the 10's of GHz, this implies an aperture size in excess of 100λ. A well-known paradigm that mitigates this challenge is multistatic sampling [4], [6], [7]. Such array topologies use transmitters and receivers that are not co-located. This allows an array with N_T transmit elements and N_R receive elements to form $N_T N_R$ spatially diverse samples. This is in contrast to a monostatic sampling scheme (wherein transmitters and receivers are co-located) which require $N_T N_R$ transmit-receive elements to achieve the same sampling.

The second challenge that the required system presents is video rate image formation. The well-known backprojection algorithm [4] can be used with any multistatic configuration, but its computational demands are extreme. Fast Fourier Transform (FFT) imaging has long been used to efficiently construct images sampled with monostatic sampling schemes [3], however, this formulation cannot be used directly with multistatic sampled data. Recently, a modified FFT imaging formulation for multistatic arrays was presented [7]. While this formulation represents a tremendous improvement over backprojection, it still requires use of multiple sub-domains and interpolations to image a human subject, adding substantial overhead to the FFT imaging formulation.

This work presents a novel multistatic array sampling scheme that allows use of the FFT-based imaging algorithm after the data undergoes a simple correction. As will be discussed, the scheme allows for high quality image reconstruction of a scene roughly the size of a human subject at video rate on COTS hardware. Fig. 1 depicts the multistatic array topology. As seen, the topology is a tiled arrangement of Boundary Arrays (BAs). The BA is a well-known sparse array layout comprised of two linear transmit arrays, and two linear receive arrays [6]. A slightly different tiled arrangement of BAs was used in [4], however, a key difference in this work is the sampling scheme. As will be discussed, the presented design samples the scene on a uniform phase center grid, with no redundancy. This is critical, as it enables the use of the presented fast imaging technique.

The next section reviews the monostatic FFT imaging for-

Distribution A: Public Release; unlimited distribution. The authors are with Massachusetts Institute of Technology Lincoln Lab-oratory, Lexington, MA, USA. This work is sponsored by the Department of Homeland Security, Science and Technology Directorate under Air Force Contract #FA8721-05-C-0002. Opinions, interpretations, recommendations and conclusions are those of the authors and are not necessarily endorsed by the United States Government.

mulation upon which this work is based. Section III discusses the novel multistatic sampling scheme and imaging algorithm, while experimental validation of the approach is presented in Section IV. Processing load of the imaging algorithm is discussed in Section V.

II. Monostatic FFT Imaging

While the presented imaging scheme employs multistatic arrays, its explanation requires discussion of monostatic FFT imaging. We consider the case where a scene is sampled with the simple quasi-monostatic imaging setup depicted in Fig. 2. As seen, the setup employs a raster scanner with two closely spaced antennas: one for transmission, one for reception. The antennas are mated to a Vector Network Analyzer (VNA), so that the frequency response of the scene is sampled on a regularly spaced two-dimensional grid. Following collection of all measurements, the image can be reconstructed with one of several techniques.

Backprojection [4] is the the simplest technique, where the image $I(\overrightarrow{r_v})$ at voxel position $\overrightarrow{r_v}$ is computed as:

$$I(\overrightarrow{r_v}) = \sum_{n_x=1}^{N_x} \sum_{n_y=1}^{N_y} s(n_x, n_y) e^{jk|\overrightarrow{r}_v - \overrightarrow{r}_T(n_x,n_y)|} e^{jk|\overrightarrow{r}_R(n_x,n_y) - \overrightarrow{r}_v|}. \quad (1)$$

It is noted that $s(n_x, n_y)$ is the matrix of measured reflections, k is the wavenumber, $\overrightarrow{r}_T$ is transmitter position, and $\overrightarrow{r}_R$ is receiver position. As the data is taken on a 2D spatial grid, n_x and n_y are column and row indices of the grid. If reflections are captured at multiple frequencies, then $I(\overrightarrow{r_v})$ is summed coherently across frequency. Backprojection is extremely computationally expensive, and becomes intractable when the measurement domain is electrically large. FFT imaging [3] is a much more efficient alternative. Using this approach, a 2D image can be formed with the following expression:

$$I(x,y) = IFFT_{2D}[FFT_{2D}[s(n_x,n_y)]e^{-j\sqrt{4k^2-k_x^2-k_y^2}z_0}] \quad (2)$$

where z_0 is the spacing between the measurement plane and the image plane. Equation (2) can, of course, be evaluated at multiple frequencies, and coherently summed within an image plane. Spatial coordinates (x, y) lie on the image plane, and correspond to the position of a sampled phase center with indices (n_x, n_y). For 3D imaging, multiple image planes can be evaluated to construct a volumetric domain in slices. Alternatively, a formulation similar to (2) using 3D FFTs can be used [3], but this requires interpolations which may be computationally expensive.

Fig. 2 provides examples of 3D images (formed in slices) constructed with (2). The images were formed using 1.25m x 1.25m scan space, sampled on a $\lambda_{hi}/2$-spaced grid at 18-26.5 GHz. Both scenes contain a metalized mannequin wearing a heavy winter coat, and a backpack concealing a can and small box. The images, which clearly show the concealed items, are color-coded according to depth of strongest return, as in [4].

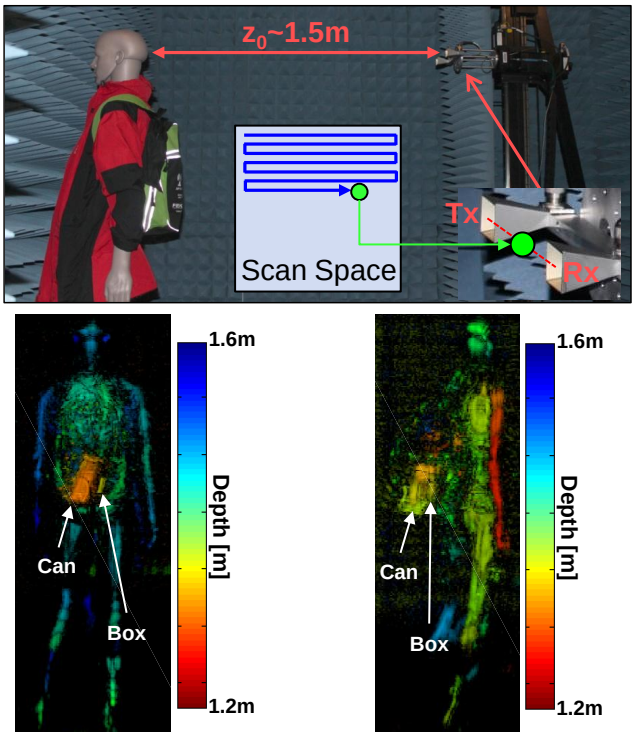

Fig. 2. Raster scanning setup for quasi-monostatic imaging and 3D images formed with setup at 18-26.5 GHz.

The preceding example used data collected with a mechanically scanning setup, though an analogous electronically switching system could be conceived for capture of a moving subject. While this would provide high quality images using an efficient reconstruction technique, it would require many transmit/receive elements (roughly 48000 for this $1.25m$ example), and is likely not an option for cost effective array implementation. In the next section, a hardware efficient multistatic scheme is examined.

III. Proposed Multistatic Imaging Scheme

Multistatic array topologies can be used to drastically reduce the number of antenna elements required in a large imaging aperture, mitigating hardware costs. Numerous multistatic aperture sampling schemes exist [4]–[7]. However, with multistatic sampling schemes, efficient reconstruction remains a challenge. While the very computationally expensive backprojection method (1) can be used for any multistatic scheme, the more efficient FFT method denoted by (2) cannot be used directly. The multistatic sampling scheme described in this section allows the FFT-based method to be used, after a very simple data correction is applied. As forthcoming results will demonstrate, the technique allows for video rate image formation on COTS computing hardware.

Fig. 1 depicts the array sampling scheme. The elementary unit of the design is the Boundary Array (BA) [6], a sparse array topology first used in ultrasonic sensing. This design employs four linear arrays that cover its perimeter. In the depicted example, the arrays on the BA's left and right side are transmitters, while the arrays on its top and bottom are

receivers. The interior of the BA is empty. Assuming that the BA is sized such that its side length is short compared to imaging range, each transmit-receive element pair forms an effective phase center, which lies at the midpoint of the two elements. If every transmit-receive pair is sampled (e.g., via rapidly switching between the elements), a grid of phase centers is formed. With exception of the missing phase centers in the grid's middle row and column, the grid is a uniformly spaced block. These missing phase centers have a negligible effect on image quality. In the depicted example, the elements are spaced by $10mm$, or 0.88λ at 26.5 GHz. The resultant phase center grid, then, is spaced by 0.44λ.

The full array topology is a tiled arrangement of BAs, as depicted in Fig. 1. Transmit-receive sampling occurs only within a given BA unit cell: in other words, a linear transmit array never communicates with a non-adjacent receive array. The result of this technique is a scene that is sampled with a regular grid of phase centers, that covers the 1.25m aperture. It is noted that each phase center is sampled only once under this configuration (i.e., the topology samples with no redundancy).

While the sampled data set lies on a regular phase center grid, it still cannot be processed with (2) until it undergoes a multistatic-to-monostatic correction. We consider the measurements as indexed in terms of the sampled 2D grid of phase centers, e.g., $s(n_x, n_y)$. Reflections for the missing phase centers in the middle row and column of each BA are set to zero. We define a reference point in the center of the imaging domain, whose position is given by $\overrightarrow{r}_{ref}$, as depicted in Fig. 3. The corrected data set is given by:

$$\hat{s}(n_x, n_y) = s(n_x, n_y) \frac{R_o(n_x, n_y)}{R_u(n_x, n_y)}. \tag{3}$$

$R_u(m, n)$ is the calculated reflection set that the multistatic design would receive if it probed a scene that contained only a point scatterer placed at $\overrightarrow{r}_{ref}$:

$$R_u(n_x, n_y) = e^{-jk|\overrightarrow{r}_T(n_x,n_y) - \overrightarrow{r}_{ref}|} e^{-jk|\overrightarrow{r}_{ref} - \overrightarrow{r}_R(n_x,n_y)|}. \tag{4}$$

$R_o(m, n)$ is the calculated reflection set that would be received by a monostatic aperture imaging the point scatterer scene, where sampling takes place on the multistatic aperture's phase center grid ($\overrightarrow{r}_c$, see Fig. 3):

$$R_o(m, n) = e^{-j2k|\overrightarrow{r}_c(n_x,n_y) - \overrightarrow{r}_{ref}|}. \tag{5}$$

The corrected data is then zero padded to size 2^N for FFT processing. In the example depicted in Fig. 1, the aperture supports a grid of 249 x 249 phase centers. While the data could be padded to 256 x 256, improved image quality was obtained with a 512 x 512 padding, and hence is used in subsequent results. The zero padded data is then processed at each frequency using (2). The process is repeated for each measured frequency, and images are summed over frequency at each depth slice in a 3D imaging domain. The imaging scheme is summarized with the block diagram depicted in Fig. 4.

It is noted that the multistatic to monostatic correction is valid over a finite imaging domain. However, as illustrated by experimental results in the next section, a single correction is sufficient for a human-sized domain. It is also noted that the correction becomes less accurate as the size of the BA tiles is increased.

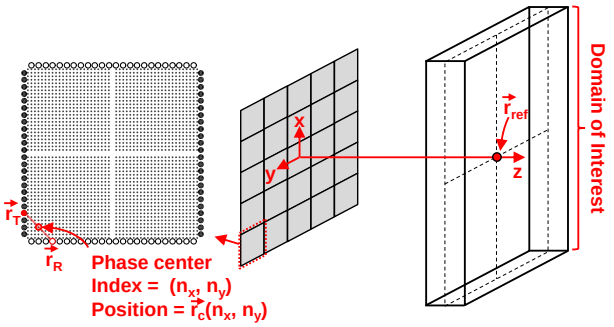

Fig. 3. Notional depiction of 5x5 tiled aperture imaging a scene.

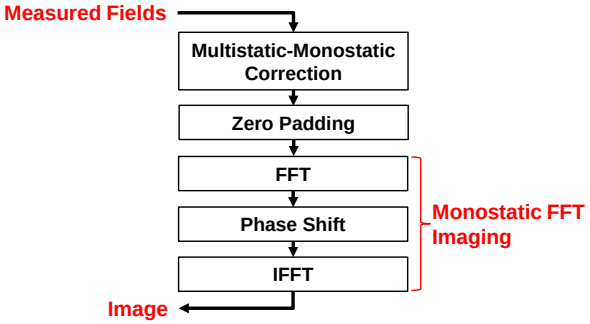

Fig. 4. Block diagram of fast multistatic imaging algorithm.

IV. Experimental Validation

To validate the sampling scheme and fast imaging algorithm, the mechanically scanning setup depicted in Fig. 5 was constructed. The system employs a Boundary Array (BA) emulator: a scanner which moves a pair of receiving antennas laterally and a pair of transmit antennas vertically. The four antennas are mated to a four port VNA. This allows for sampling of the scene in the same manner as the BA. The BA emulator is placed on an x-y scanner, allowing for acquisition of the tiled boundary array setup depicted in Fig. 1. It is noted that, due to the size of the waveguide antennas used in the setup, the closest transmit-receive pairs could not be measured. Nevertheless, high quality images were still formed with the setup.

Reconstructed images acquired with the setup are depicted in Fig. 6. In one of the two images, the imaged scene contains a metalized mannequin concealing a small metal tube under a heavy coat, while in the other, the dummy conceals a can and small box in a backpack. In both cases the concealed objects are clearly visible. Both images were formed with 18-26.5 GHz stimulus, using 160 frequency points. The 3D images were realized with 21 depth slices, spaced by 0.015m. Fig. 7 depicts the same two scenes, formed at 23.6-26.5 GHz, using 56 frequency steps.

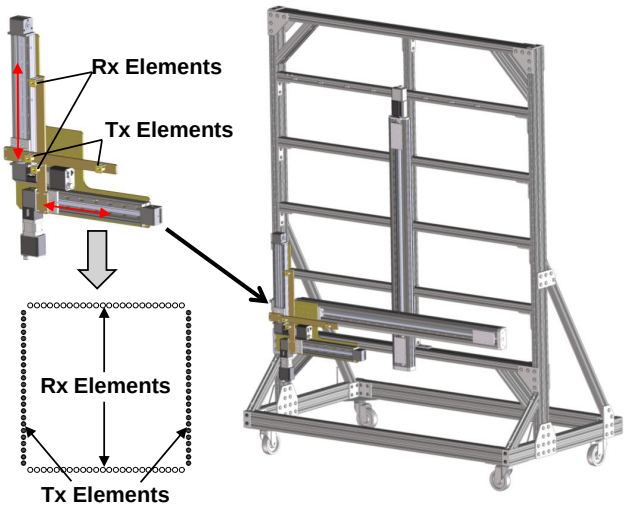

Fig. 5. Mechanically scanning multistatic array emulator for validation of sampling scheme.

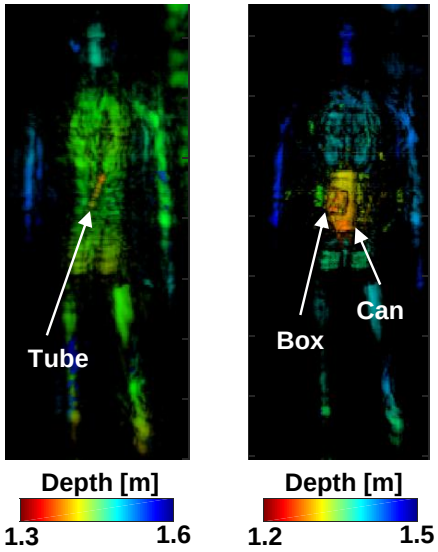

Fig. 6. Reconstructed images at 18-26.5 GHz (160 frequency steps) acquired with setup depicted in Fig. 5. Formation time on cluster of COTS GPUs was 0.101sec.

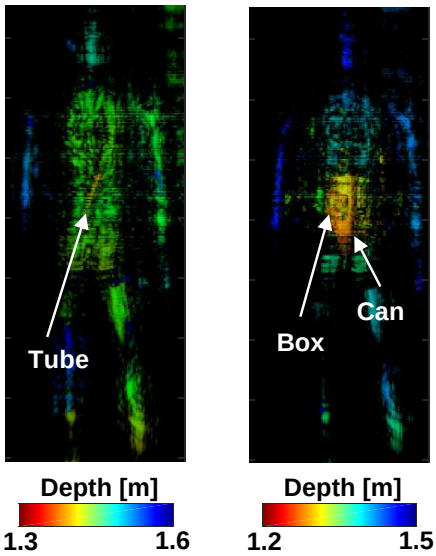

Fig. 7. Reconstructed images at 23.6-26.5 GHz (56 frequency steps) acquired with setup depicted in Fig. 5. Formation time on cluster of COTS GPUs was 0.048sec.

V. Computational Load

For real time imaging capability, image reconstruction must occur at video rate. The technique presented in the previous section provides a reconstruction solution that is orders of magnitude faster than backprojection, and can operate at video rate using COTS computing hardware. The complexity of the algorithm was evaluated using computational workload values provided in [8]. The resulting load (in GFLOPS, or billion Floating Point Operations per Second) is plotted in Fig. 8. For comparison, the load of the backprojection technique is also plotted. In that analysis, it is assumed that only the domain roughly occupied by the dummy (1.9m x 0.6m x 0.3m, discretized by 1cm) is of interest. As seen, the FFT technique is roughly two orders of magnitude less computationally intensive than the backprojection technique. For 10 Hz operation with 160 frequency points, the FFT method's load is about 1409 GFLOPS, while backprojection requires 174532 GFLOPS. If 56 frequency points are used at 10 Hz, the loads of the FFT and backprojection methods are 493 GFLOPS and 61148 GFLOPS, respectively.

A COTS computer with four Nvidia GeForce Titan X Graphics Processing Units (GPUs) was used to reconstruct images using the FFT technique. For the imaging scenario presented in Fig. 6 (512 x 512 FFT size, 160 frequency points, 21 depth slices), computation time was observed as 0.101sec. For the 56 frequency point case depicted in Fig. 7, the computation time was observed as 0.048sec. These results illustrate that real time image reconstruction of a human-sized domain is possible using the presented technique, with COTS computing hardware.

VI. Conclusions

A novel multistatic array topology and efficient FFT-based imaging algorithm have been presented. The array employs a tiling of Boundary Arrays (BAs) to sample the scene on a uniform grid of phase centers. After a simple correction is applied, image reconstruction can be performed using the highly efficient FFT imaging technique. The method was validated experimentally, and was shown to form high quality microwave images. Computational complexity analysis shows that the technique is roughly two orders of magnitude less computationally demanding than backprojection. Further, the scheme was shown to render a 3D image in 0.048sec-0.101sec (depending on number for frequency points used) on a cluster of four COTS GPUs.

VII. Acknowledgment

The authors thank Edward Martin for measurement support. Additionally, the authors thank David Bragdon, Anthony Mormile, Peter Priestner and Thomas Matte for mechanical

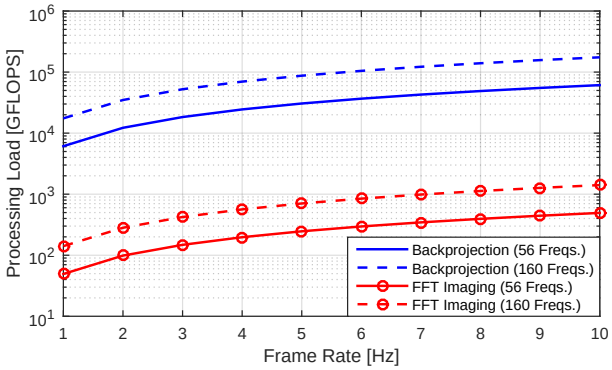

Fig. 8. Computational complexity of multistatic FFT imaging scheme, compared with backprojection.

design and assembly support. This work was supported by the Department of Homeland Security, Science and Technology Directorate under Air Force Contract FA8721-05-C-0002.

REFERENCES

[1] M. T. Ghasr, M. A. Abou-Khousa, S. Kharkovsky, R. Zoughi, and D. Pommerenke, "Portable real-time microwave camera at 24 ghz," *IEEE Transactions on Antennas and Propagation*, vol. 60, no. 2, pp. 1114–1125, 2012.

[2] E. C. Fear, X. Li, S. C. Hagness, and M. A. Stuchly, "Confocal microwave imaging for breast cancer detection: Localization of tumors in three dimensions," *IEEE Transactions on Biomedical Engineering*, vol. 49, no. 8, pp. 812–822, 2002.

[3] D. M. Sheen, D. L. McMakin, and T. E. Hall, "Three-dimensional millimeter-wave imaging for concealed weapon detection," *IEEE Transactions on Microwave Theory and Techniques*, vol. 49, no. 9, pp. 1581–1592, 2001.

[4] S. S. Ahmed, A. Schiessl, F. Gumbmann, M. Tiebout, S. Methfessel, and L. Schmidt, "Advanced microwave imaging," *IEEE Microwave Magazine*, vol. 13, no. 6, pp. 26–43, 2012.

[5] B. Gonzales-Valdes, C. Rappaport, and J. A. Martinez-Lorenzo, "On-the-move active millimeter wave interrogation system using a hallway of multiple transmitters and receivers," 2014, pp. 1107–1108.

[6] R. J. Kozick and S. A. Kassam, "Synthetic aperture pulse-echo imaging with rectangular boundary arrays," *IEEE Transactions on Image Processing*, vol. 2, no. 1, pp. 68–79, 1993.

[7] Y. Alvarez, Y. Rodriguez-Vaqueiro, B. Gonzalez-Valdes, S. Mantzavinos, C. M. Rappaport, F. Las-Heras, and J. A. Martinez-Lorenzo, "Fourier-based imaging for multistatic radar systems," *IEEE Transactions on Microwave Theory and Techniques*, vol. 62, no. 8, pp. 1798–1810, 2014.

[8] M. Arakawa, *Computational Workloads for Commonly Used Signal Processing Kernels*, ser. Project report, MIT Lincoln Laboratory, 2006. Lincoln Laboratory, Massachusetts Institute of Technology, 2003.